TECHNICAL PAPER

Effect of sputtering power on friction coefficient and surface energy of co-sputtered titanium and molybdenum disulfide coatings and its performance in micro hot-embossing

**B. Saha · M. Dirckx · D. E. Hardt ·
S. B. Tor · E. Liu · J. H. Chun**

Abstract Si micromolds are common for fabrication of polymer-based microfluidic devices by hot-embossing because of the well established fabrication methods for Si, e.g., deep reactive ion etching, for favorable surface finish and accuracy. The problems with low yield, poor reproducibility, premature failure and limited lifetime of a Si micromold are induced by high friction and surface adhesion generated during demolding. Therefore, Titanium (Ti) and molybdenum disulfide (MoS_2) coatings were deposited on Si micromolds via magnetron co-sputtering at various combinations of target powers to improve its surface properties. Coating composition, crystallographic orientation, roughness, critical load, hardness, friction coefficient and surface energy were measured by X-ray photoelectron spectroscopy, X-ray diffraction, atomic force microscopy, scratch testing, nanoindentation, ball-on-disc tribometry and the contact angle method respectively. A statistical design of experiment matrix was used to investigate the effect of the Ti and MoS_2 target powers on the friction coefficient and surface energy of the coatings. From this designed experiment, it was observed that increasing MoS_2 target power was associated with increasing surface energy and decreasing friction coefficient and target powers had statistically significant effects on these parameters. Crystallinity, roughness and hardness of the coatings increased with increasing Ti concentration. A mathematical model of the effects of Ti and MoS_2 target powers on the friction coefficient and surface energy of the coatings has been fit to the experimental results using the response surface method. Uncoated and MoS_2–Ti coated Si micromolds were used in hot-embossing for a comparative study on replication performance of uncoated and various coated micromolds. Hotembossed PMMA microstructures showed that coating improve replication performance of Si micromolds. Si micromold coated with co-sputter of Ti and MoS_2 at power of 300 and 75 W respectively, showed better replication quality among the selected target powers.

1 Introduction

Tribological properties such as friction and adhesion are involved in all moving parts. Following modern technological trends toward miniaturization with dimensions measured at the micro/nano-scale, the effect of these surface properties have become more prominent (Stoldt and Bright 2006).

Si is the most widely used material for the production of miniaturized mechanical components and devices (for example, micro-electromechanical system or MEMS) because complex micro-scale structures can be produced using well-established lithographic patterning and etching methods. Unfortunately, Si has poor mechanical and tribological properties, which precludes its use in systems that experience extensive sliding and rolling contact (Smallwood et al. 2006; Radhakrishnan et al. 2002; Patton and Zabinski 2002). The high brittleness, adhesion force

B. Saha · S. B. Tor (✉)
Singapore-MIT Alliance, Nanyang Technological University,
65 Nanyang Avenue, Singapore 637460, Singapore
e-mail: msbtor@ntu.edu.sg

M. Dirckx · D. E. Hardt · J. H. Chun
Department of Mechanical Engineering,
Singapore-MIT Alliance, Massachusetts Institute of Technology,
77 Massachusetts Avenue, Cambridge, MA, USA

S. B. Tor · E. Liu
School of Mechanical and Aerospace Engineering,
Nanyang Technological University, 50 Nanyang Avenue,
Singapore 639798, Singapore

and friction coefficient of Si reduce system lifetime and rule out the use of motion limit structures such as micromotors or microgears. Practical micro-devices made of Si must be designed to circumvent these limitations. In order to achieve the full potential of micro-devices, it is necessary to modify silicon's surface properties to survive under conditions of significant rolling and sliding contact and extreme environments.

Silicon has also found wide use as a mold material in several micro-scale molding processes including hot embossing (Becker et al. 1999; Esch et al. 2003), injection molding (Loke et al. 2007), micro powder injection molding (Fu et al. 2007), and nanoimprint lithography (Schift 2008). Silicon's poor tribological properties can cause defects when separating the part from the mold (demolding) (Hirai et al. 2003; Hsueh et al. 2006; Fu et al. 2008; Dirckx 2010). Several researchers have attempted to improve the tribological performance of silicon micromolds by applying surface coatings, including fluoropolymers (Hirai et al. 2001; Yeo et al. 2006; Gao et al. 2006) and hard coatings (Saha et al. 2009, 2010a, b). Because fluoropolymer coatings have been found to have limited lifetime (Jaszewski et al. 1999), hard coatings have the greatest promise for improving the performance of silicon micromolds.

This work is aimed at improving the performance of silicon micromolds for producing polymeric microfluidic chips by applying anti-sticking MoS_2 and Ti coatings by DC magnetron co-sputtering. A combination of low friction coefficient and surface energy with high wear resistance make MoS_2–Ti coatings suitable for a number of applications such as in aerospace, dry machining, ball bearings and others (Hilton and Fleischauer 1992; Spalvins 1974; Renevier et al. 2000). These properties also make MoS_2–Ti a promising candidate for micromold coatings. A clear understanding of the effects of deposition parameters on tribological properties such as coefficient of friction and surface energy is needed to facilitate the wider use of MoS_2–Ti for micromolds.

Some researchers have studied the effect of relative percentage of Ti and MoS_2 in MoS_2–Ti coatings in a traditional experimental design approach by varying one factor while keeping other factors constant (Gangopadhyay et al. 2009; Rigato et al. 1999, 2000). While this approach is simple in execution, it does not address the complex relationship among deposition parameters and tribological properties. This approach also contributes little understanding of the process robustness. The statistical design of experiments approach is an effective method for investigating the effects and importance of many variables and their interactions in a complex process (Dirckx 2010; Wilson and Sullivan 2007; Ma et al. 2007). In this work, a response surface analysis approach is used to systematically study the main and interaction effects of MoS_2 and Ti

target power on the friction coefficient and surface energy of deposited coatings. This approach permits the development of mathematical models that relate process parameters to coating properties, enabling better process control and optimization.

2 Experimental

2.1 Design

A full factorial experimental design was carried out to evaluate the combined effects of process variables on the friction coefficient and surface energy of deposited coatings. This full factorial experimental design plan used MoS_2 and Ti target power as process variables. Settings for these are shown in Table 1. Operating windows for target power were chosen based on the limits of the sputtering machine, understanding of the sputtering process and some preliminary trial runs. To check for nonlinear effects and to enable quadratic model fitting, a three-level design was selected. With three levels of two variables, a full factorial design requires nine different combinations of experimental parameters. Three replicates were preformed for each combination of deposition parameters, for a total of twenty-seven experimental runs. Measurements of the properties of each deposited sample were repeated three times to ensure the reliability of the data. Statistical analysis was done using Minitab version 15 to perform regression analysis of the data and to estimate the coefficients of a quadratic model. Such a model is presented in Eq. 1,

$$y = \beta_0 + \sum_{i=1}^{k} \beta_i x_i + \sum_{i=1}^{k} \beta_{ii} x_i^2 + \sum \sum_{i<j} \beta_{ij} x_i x_j + \varepsilon \qquad (1)$$

where, y, β_0 and ε are the measured response, intercept and error term, respectively. β_i, β_{ii} and β_{ij} are the coefficients of the 1st order, 2nd order and interaction effects of the variables, x_i, x_j respectively.

2.2 Deposition of coatings

Silicon micromolds of 3.2×2 cm^2 containing arrays of raised features 100 μm in height and width with a spacing of 500 μm were used as a deposition substrate. The MoS_2–Ti coatings were deposited by using magnetron co-sputtering (AJA Orion 5) that using MoS_2 (MoS_2, 99.99 %) and Ti (Ti, 99.99 %) as target materials at a pressure of about 3 mTorr for 60 min. Before they were introduced into the deposition chamber, the silicon micromolds were first rinsed with deionised (DI) water and methanol alternately for eight times to remove potential contaminants, followed by ultrasonic cleaning in ethanol for 20 min at 30 °C. Prior

Table 1 Sputtering powers on Ti and MoS_2 targets used during sputtering deposition, Ti, Mo, S and O concentrations, friction coefficient and surface energy of various MoS_2–Ti coatings

Samples	MT1	MT2	MT3	MT4	MT5	MT6	MT7	MT8	MT9
Ti (W) target power	300	275	250	300	275	250	300	275	250
MoS_2 target power (W)	50	50	50	75	75	75	100	100	100
Friction coefficient	0.435	0.394	0.366	0.302	0.284	0.261	0.229	0.220	0.194
	0.416	0.387	0.364	0.283	0.288	0.254	0.218	0.216	0.187
	0.423	0.386	0.350	0.282	0.270	0.248	0.212	0.208	0.184
Surface energy (dyne/cm)	15.62	15.39	16.82	20.61	30.26	38.41	41.52	46.8	55.88
	15.52	15.68	17.39	20.13	30.49	38.15	41.79	45.9	55.76
	15.77	15.55	16.68	20.47	30.41	38.19	41.98	44.89	56
Ti (at.%)	46.1	45.5	44.9	42.6	39.8	36.7	36.8	36.0	35.2
Mo (at.%)	16.1	17.6	18.1	21.0	25.3	28.8	29.6	29.8	31.2
S (at.%)	14.0	14.3	14.3	15.8	17.9	20.8	22.6	22.8	22.8
O (at.%)	23.7	22.6	22.7	20.6	17.0	13.8	11.0	11.4	10.8

to depositions, substrates were etched inside the sputtering chamber by argon (Ar) plasma for 20 min at a pressure of about 20 mTorr and a substrate bias of −250 V. During the depositions, Ar gas was introduced into the deposition chamber at a fixed flow rate of 12 sccm at 0 V substrate bias. During all deposition runs, the samples were kept at the center of the sample holder and were rotated at 20 rpm to maintain the uniformity of the coatings.

2.3 Fabrication of polymer balls

Polymethyl methacrylate (PMMA) (MH; Tecnik Polymers and Colourants) balls of 6 mm diameter were fabricated by injection molding (IM) to measure the friction coefficient between PMMA and different coated surfaces. The melt mass-flow rate, specific gravity and glass transition temperature of PMMA are 2 g/10 min, 1.19 and 115 °C respectively. The material was pre-dried at 90 °C for 5 h using a dehumidifying drier before molding. Process parameters such as injection temperature, pressure velocity and mold temperature were 310 °C, 1100 bar, 900 ccm/s and 80 °C respectively, which were chosen based on the previous work (Saha et al. 2010).

2.4 Characterization

Coating thicknesses were measured using a KLA-Tencor profiler and XRD measurements were performed using a CuKα line source for 12.5°–80°.

X-Ray photoelectron spectroscopy (XPS) was used to study the chemical states of the coated samples using a monochromatic Al Kα excitation. Actual coating compositions were evaluated by surface etching for 15 min inside the XPS chamber.

Hardness and elastic modulus were determined by nanoindentation. Indentation depth was 150 nm with an allowable drift rate of 0.1 mm/s, and the frequency of indentation was 45 Hz.

Atomic force microscopy (AFM) (CSPM-4000) with a silicon nitride cantilever was used in tapping mode to study the surface morphology and roughness of the coatings under ambient atmospheric conditions inside a close chamber with a scanning rate of 0.7 Hz and a scan area of 5 μm × 5 μm.

Scratch tests were performed using a microscratch tester (SST-101, Shimadzu) with a diamond tip of 15 μm radius, where the diamond stylus was pulled over the sample surface in a progressive loading mode with a scratch rate of 10 μm/s. This test was performed to quantify the adhesive strength between the coating and the substrate by evaluating the minimum normal load required to delaminate the coating, which is referred as the critical load.

The friction coefficient of the coatings was measured with a ball-on-disc microtribometer (CMS™) at room temperature using a PMMA ball of 6 mm in diameter. The balls were slid on each sample surface for 250 laps along a track of 1 mm in radius at a sliding speed of 5 cm/s and normal load of 1 N in.

Contact angles were measured with DI water and ethylene glycol droplets to determine the surface energies of the various coatings. The average value of three measurements was taken to calculate surface energy for each sample.

Microfluidic devices were fabricated by MIT own built hot-embossing setup using uncoated and coated micromold (Barletta et al. 2006). Hot-embossing process is described elsewhere (Saha et al. 2010a, b).

3 Results and discussion

Measured thicknesses of the coatings were in the range from 500 to 700 μm depending on the variation of Ti and MoS_2 target power. Higher target power leads to a thicker coating.

Atomic percentages of elements in different coatings were found from their integrated net intensities in XPS spectra, which are listed in Table 1. The atomic percentages vary depending on the relative power of the targets.

Figure 1 shows XRD results for the nine different experimental conditions. Two XRD peaks at around 40°–70° are observed, which correspond to the MoS_2 (103) and Ti (103), respectively (Ma et al. 2009; Firouzi-Arani et al. 2010). Full with at half maximum (FWHM) of the peak is inversely related to the crystal size (Kahraman et al. 2005). A very sharp, narrow Ti XRD peak is observed when the relative percentage of the Ti target is higher. The FWHM of the Ti XRD peak increases along with the relative MoS_2 target power. This result implies that Ti is able to form large crystals when its relative atomic percentage is higher, while incorporation of MoS_2 disturbs the crystallization of the Ti matrix. An increase in MoS_2 peak height is observed with increasing MoS_2 target power because of the increase in the MoS_2 concentration.

The surface roughness of the coatings increases with higher relative percentage of MoS_2 target power, as shown in Fig. 2. This phenomenon can be explained from the XRD results. The crystallinity and uniformity of the Ti matrix has been disturbed by the introduction of MoS_2, as indicated by the broadening of the Ti peak. At the same time, MoS_2 also forms extra grains at higher relative MoS_2 target power, which causes an increase in the surface roughness.
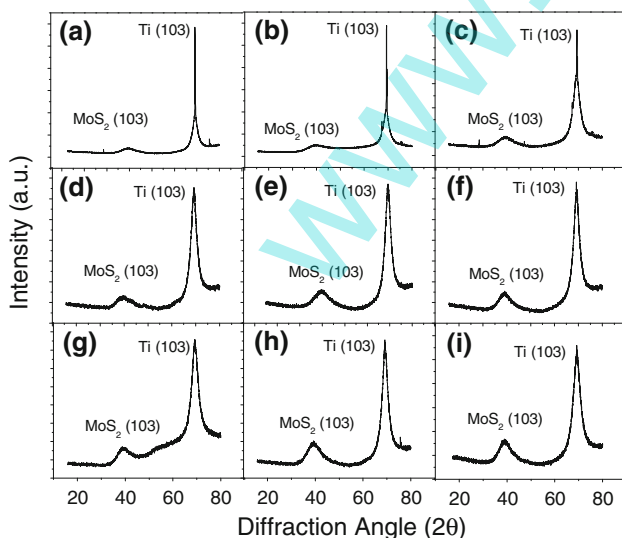

Fig. 1 XRD patterns of a MT1, b MT2, c MT3, d MT4, e MT5, f MT6, g MT7, h MT8 and i MT9 coatings
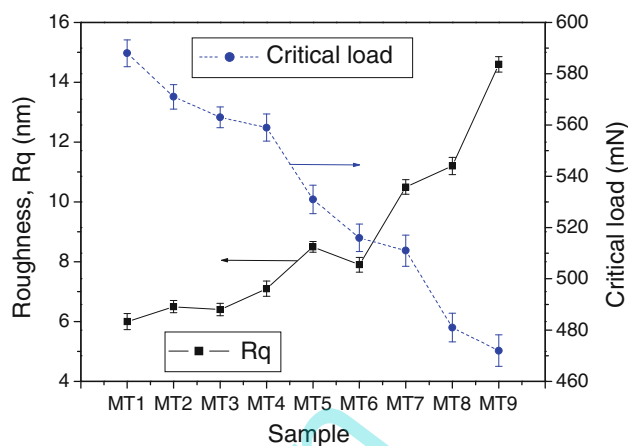

Fig. 2 Roughness (Rq) and critical load of MoS_2–Ti coatings

The critical loads of different coatings are presented in Fig. 2. Critical load gives a quantitative measure of the adhesive strength between the coating and substrate materials. Other researchers have evaluated the relation between residual stress, hardness with the critical load (Benjamin and Weaver 1960; Benayoun et al. 1999). Ichimura and Rodrigo (2000) experimentally found that critical load is proportionally related to the hardness of the coatings. Residual stress is generated from the structural mismatch, growth induced stress and thermal stress. Since the crystal structures of the coatings deposited in this study are almost the same (as shown in the XRD results) and deposition was done at room temperature, the residual stresses for these coatings are almost the same. Therefore, in this case the critical load is mainly influenced by the hardness of the coatings, which depends on the relative percentage of Ti and MoS_2 target power. Figure 2 shows a continuous increase of critical load with increasing Ti content. A large amount of small chips are observed in coatings containing a higher percentage of Ti, whereas larger spallation is observed in the coatings with higher content of MoS_2. This observation indicates that coatings with higher Ti content are harder and more brittle, while coatings with higher MoS_2 content are softer.

Load–displacement indentation plots for the different coatings are shown in Fig. 3. The maximum applied load varies from 1.5 to 5.5 mN, depending on the hardness of the coatings. Hardness values are on the order of MT1 (20.1 GPa) > MT2 (14 GPa) > MT3 (12.9 GPa) > MT4 (9.5 GPa) > MT5 (9.3 GPa) > MT6 (7.4 GPa) > MT7 (5.7 GPa) > MT8 (5.2 GPa) MT9 (3.8 GPa). Since Ti is harder than MoS_2, the hardness of the coatings increases with the Ti concentration.

The Ti and MoS_2 target powers vary from 50 to 100 W and 250 to 300 W, respectively. Over the above ranges of target power, the friction coefficient ranges from 0.18 to
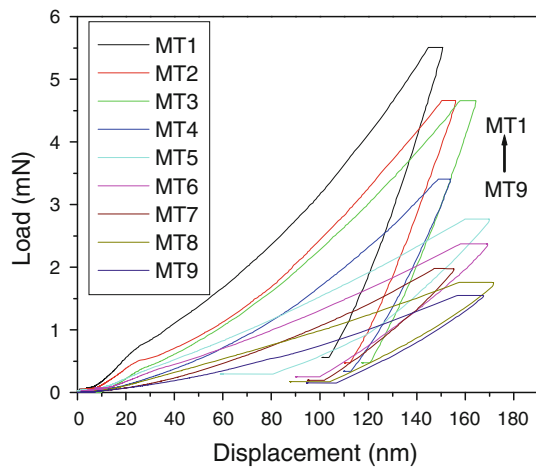
Fig. 3 Load–displacement curves from nanoindentation tests of various MoS$_2$–Ti coatings

Table 2 Regression of coefficients of friction and surface energies

	Term	Coef	SE coef	t-ratio (t)	Probability (p)
Friction coefficient	Constant	0.278	0.004	74.6	0
	Ti	0.022	0.002	10.7	0
	MoS$_2$	−0.092	0.002	−44.9	0
	Ti × Ti	−0.005	0.004	−1.5	0.139
	MoS$_2$ × MoS$_2$	0.025	0.004	7	0
	Ti × MoS$_2$	−0.008	0.003	−3.3	0.003
Surface energy (dyne/cm)	Constant	29.089	1.034	28.1	0
	Ti	−5.548	0.566	−9.8	0
	MoS$_2$	15.894	0.566	28.1	0
	Ti × Ti	0.886	0.981	0.9	0.377
	MoS$_2$ × MoS$_2$	2.261	0.981	2.3	0.031
	Ti × MoS$_2$	−3.198	0.694	−4.6	0

0.43, as shown in Table 1. The results of the response surface regression using a central composite design are presented in Table 2. All the terms of the regression model related to MoS$_2$ target power are highly significant, as values of the t-ratio (coefficient to standard error) and p (probability) are very large and small respectively. The higher order term related to Ti target power does not play a significant role, as their p value is very high. The calculated values of R^2 and R^2 (adjusted) were 99.1 and 98.8 % respectively, which indicate a strong correlation between the observed and predicted values of the response.

Analysis of variance (ANOVA) results are presented in Table 3. These results also suggest that the regression model is highly significant as the calculated Fishers's f and probability p of the regression are 438.73 and 0.0 respectively. A large value of f indicates that variation of the

response can be explained by the regression equation, and the associated p indicates the significance of the large f value. The p value is used to verify the significance of the coefficients of the regression model (Eq. 1) through testing the 'null hypothesis' (H$_0$ hypothesis). In common practice, a confidence level of 95 % (corresponding to a p value <5 %) is considered significant. The H$_0$ hypothesis is thus rejected and the factor is considered to have a significant influence when $p \leq 0.05$. On the sole condition that $p \leq 0.05$, the variance explained by the model is significantly larger than the unexplained variance. The polynomial quadratic model (second order response surface model) obtained by multivariate regression is as follows:

$$\mu = -0.39703 + 0.00666 \times Ti - 0.00594 \times MoS_2$$
$$- 8.711 \times 10^{-6} \times Ti^2 + 3.955 \times 10^{-5} \times MoS_2^2$$
$$- 1.333 \times 10^{-5} \times Ti \times MoS_2 \qquad (2)$$

Where μ, Ti and MoS$_2$ represent friction coefficient, titanium target power and molybdenum disulfide target power respectively. The validity of assuming a normal distribution of the data sets was examined by the graphical technique, for which the normal probability plots are shown in Fig. 4a. A good alignment of the data close to a straight line is observed, which suggests that the data are normally distributed. The histogram of the residuals in Fig. 4b shows an almost symmetrical distribution. Figure 4c shows a plot of the residuals versus the fitted values. The data are scattered randomly along both sides of the zero line without any pattern, and no predominance of positive or negative residuals can be observed. Randomization in scattering is also observed in Fig. 4d. All these results indicate a highly significant model fit. Figure 5 shows the response surface for friction coefficient with respect to the Ti and MoS$_2$ target powers. It can be seen that friction coefficient gradually decreases with the MoS$_2$ power, and increases with Ti power. MoS$_2$ act as a solid lubricant and since the percentage of MoS$_2$ in the coating increases with the MoS$_2$ target power, the friction coefficient of the coatings decreases with the MoS$_2$ target power (Donnet 1996; Xu et al. 2003). From the surface profile plot it is also observed that, for a constant Ti power, friction coefficient decreases with increasing in MoS$_2$ target power. This is because of the solubility of Ti in the MoS$_2$ matrix increases with the MoS$_2$ concentration (Renevier et al. 2000), which causes a decrease in the friction coefficient of the coatings.

The surface energy of the coatings was determined by measuring the contact angle using water and ethylene glycol. Young's equation represents the relation between the contact angle and surface energy, as shown in Eq. 3 (Saha et al. 2010a; Owens and Wendt 1969).

Table 3 Design parameters for friction coefficient and surface energy

	Source	df	Seq SS	Adj SS	Adj MS	f	Probability (p)
Friction coefficient	Regression	5	0.165	0.165	0.033	438.73	0
	Linear	2	0.160	0.160	0.080	1065.73	0
	Square	2	0.004	0.004	0.002	25.56	0
	Interaction	1	0.001	0.001	0.001	11.08	0.003
	Residual error	21	0.002	0.002	0.000		
	Pure error	18	0.001	0.001	0.000		
	Total	26	0.167				
Surface energy (dyne/cm)	Regression	5	5259.6	5259.6	1051.9	182.24	0
	Linear	2	5101.5	5101.5	2550.8	441.90	0
	Square	2	35.4	35.4	17.7	3.07	0.068
	Interaction	1	122.7	122.7	122.7	21.25	0
	Residual error	21	121.2	121.2	5.8		
	Pure error	18	2.5	2.5	0.1		
	Total	26	5380.8				

Fig. 4 **a** Normal probability of residuals, **b** histogram of residuals, **c** residual versus fitted data and **d** residual versus order of data for friction coefficient
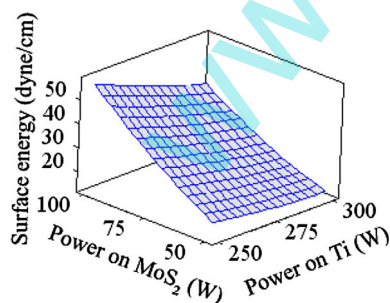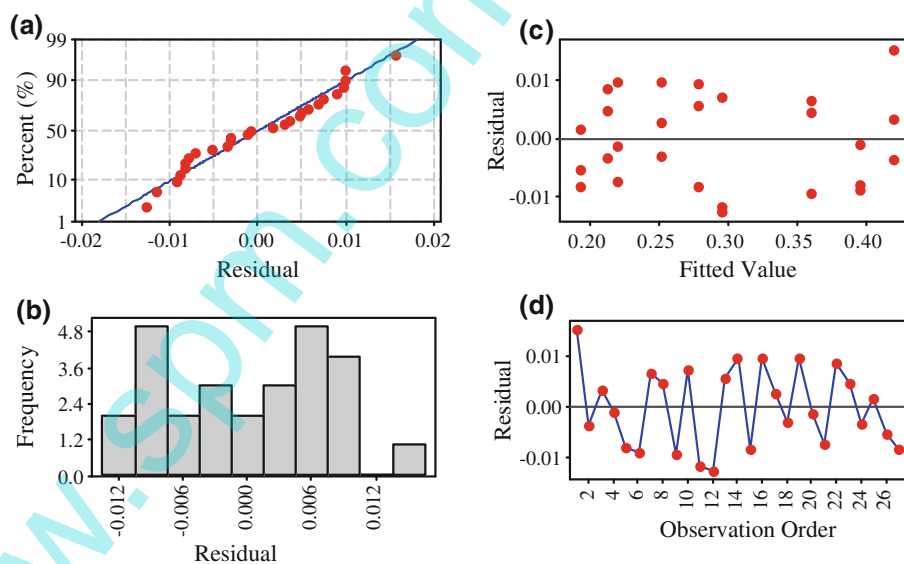
Fig. 5 Combined effect of MoS$_2$ and Ti target powers on friction coefficient of MoS$_2$–Ti coatings

$$\gamma_{sv} = \gamma_{sl} + \gamma_{lv} \cos \theta + \pi_e \qquad (3)$$

where γ_{sv}, γ_{lv} and γ_{sl} are the free energies against vapor of the solid, liquid and interface respectively, θ is the measured contact angle and π_e is an equilibrium pressure of the adsorbed vapor on the solid, which are assumed to be zero in this case.

Surface and interface energies have two components that are related through the following equations:

$$\gamma_{sv} = \gamma_{sv}^d + \gamma_{sv}^p \qquad (4)$$

$$\gamma_{lv} = \gamma_{lv}^d + \gamma_{lv}^p \qquad (5)$$

$$\gamma_{sl} = \gamma_{sl}^d + \gamma_{sl}^p \tag{6}$$

$$\gamma_{sl}^d = \gamma_{sv}^d + \gamma_{lv}^d - 2\left(\gamma_{sv}^d \times \gamma_{lv}^d\right)^{1/2} \tag{7}$$

$$\gamma_{sl}^p = \gamma_{sv}^p + \gamma_{lv}^p - 2\left(\gamma_{sv}^p \times \gamma_{lv}^p\right)^{1/2} \tag{8}$$

After combining these equations, one obtains the relation between the dispersive and polar force with contact angle as presented in Eq. 9:

$$(1 + \cos\theta)\left(\gamma_{lv}^d + \gamma_{lv}^p\right) = 2\left(\gamma_{sv}^d \times \gamma_{lv}^d\right)^{1/2} + 2\left(\gamma_{sv}^p \times \gamma_{lv}^p\right)^{1/2} \tag{9}$$

The surface energies of the different coatings were calculated from Eq. 9. The dispersive (γ_{lv}^d) and polar (γ_{lv}^p) components of surface energy for DI water are 21.8 and 51 dyne/cm, respectively. The dispersive and polar components for ethylene glycol are 29.3 and 19 dyne/cm respectively (Saha et al. 2009, 2010a).

As with the friction coefficient, the influence of Ti and MoS_2 target power on the surface energy were determined by regression analysis based on the experimental data presented in Table 1. The fitted response from the experimental data is shown in Eq. 10:

$$s = 64.4895 - 0.618011 \times Ti - 1.50001 \times MoS_2 \\ + 0.00141 \times Ti^2 + 0.00361778 \times MoS_2^2 - 0.005116 \\ \times Ti \times MoS_2 \tag{10}$$

Where s represents surface energy of the coatings. The estimated coefficients for the response surface regression and the analysis of variance results are presented in Table 2 and Table 3 respectively. The small value (<0.05) of probability p for most of the parameters indicates a good fit between the regression model and the measured surface

energies. A larger probability value of 0.377 for the second order Ti target power effect is observed, which indicates that this higher order effect does not play a significant role in determining the surface energy of the coatings. The high value of the determination coefficient, R^2 (97.75) suggest that the model explains 97.75 % of the variation in the observed response.

A good alignment of data along the straight line in Fig. 6a and almost equal scatter on both side of the straight line in Fig. 6b, c is also observed, providing further evidence for the validity of the regression model. Figure 7 shows the relation of the Ti and MoS_2 target power with the surface energy. From this plot it can be seen that the effect of the MoS_2 target power is more pronounced compared to that of the Ti target power. Surface energy increases with the MoS_2 and decreases with the Ti target power.

Because of high adhesion and friction force, the uncoated micromold cannot be used for repetitive numbers of replication. Performance of uncoated and various MT
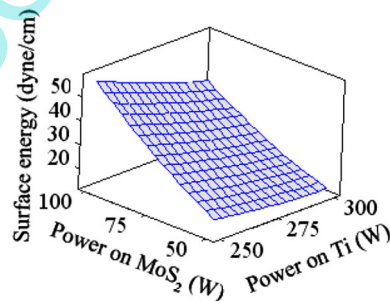
Fig. 7 Combined effect of MoS_2 and Ti target powers on surface energy of MoS_2–Ti coatings

Fig. 6 **a** Normal probability of residuals, **b** histogram of residuals, **c** residual versus fitted data and **d** residual versus order of data for surface energy
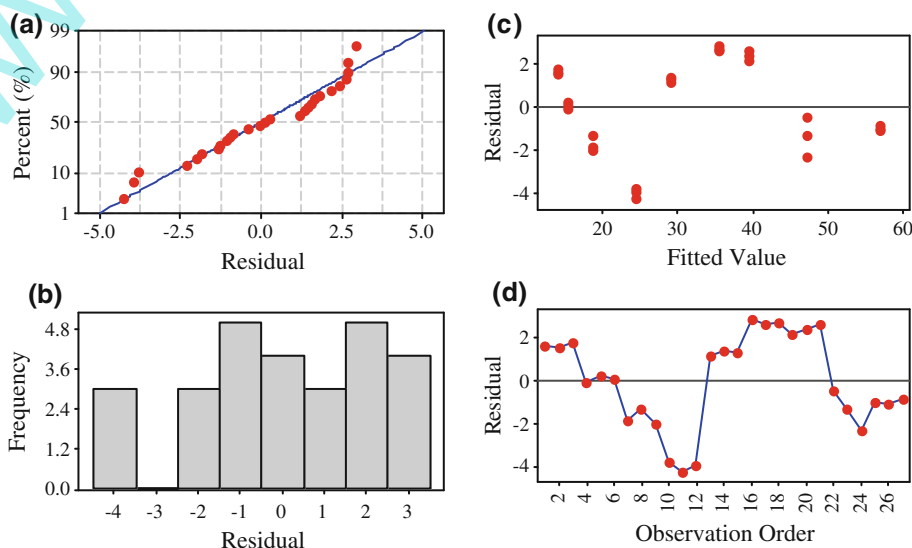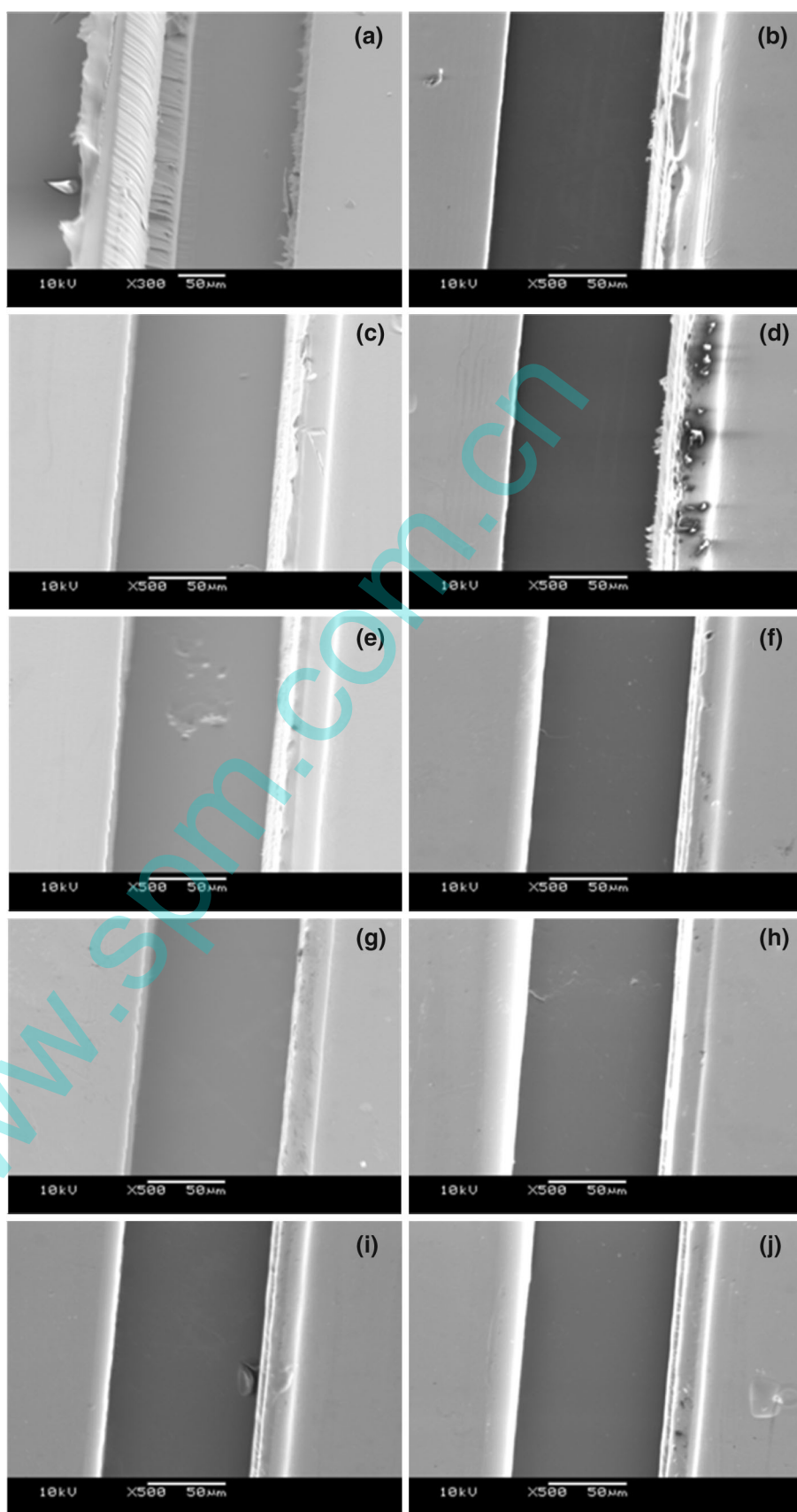
Fig. 8 SEM micrographs of demolded PMMA products from **a** bare Si mold and **b** MT9, **c** MT8, **d** MT7, **e** MT6, **f** MT5, **g** MT4, **h** MT3, **i** MT2 and **j** MT1 coated Si molds

coated Si micromolds was studied by hot-embossing to fabricate PMMA microfluidic device. Figure 8 shows PMMA microstructures after first hot-embossing. Damage and improper replication on the sidewall of the PMMA channel are observed using uncoated Si micromold as shown in Fig. 8a. Improvement in finishing at sidewall of the microchannels is observed using MT coated micromolds as shown in Fig. 8b–j. Distortion at the sidewall of the microchannels fabricated using MT9 to MT4 coated micromold continuously decreases. MT4 coated micromold shows better replication as compare to other coatings. According to Table 1, surface energy decreases from MT9 to MT1 therefore adhesion between PMMA and micromold decreases, which improves replication performance from MT9 to MT4 coated Si micromold. At the same time, coefficient of friction increases from MT9 to MT1 which further increases distortion at side wall of PMMA channels fabricated using MT3 and MT1 coated microchannels.

4 Conclusions

In this paper, an attempt was made to find the effect of sputtering power on the properties such as crystallinity, roughness, hardness and critical load of co-sputtered MoS_2–Ti coatings. Complex relationships between the friction coefficient and surface energy and the target power using a statistical design of experiment method were also investigated. The concentration of Ti and MoS_2 in the coating depends on their relative target powers and the composition of the coatings influences their properties. Roughness and critical load of the coatings increases and decreases respectively with increasing relative percentage of MoS_2 target power. The coating labeled MT9 coating has a highest surface roughness (Rq) of 14.6 nm and the lowest critical load of 472 mN. The hardest coating, labeled MT1 coating, contains the highest percentage of Ti. The fitted response surface model indicates that the Ti and MoS_2 target powers both have a significant effect on the friction coefficient and the surface energy. The higher order term related to the Ti target power does not have a significant effect on the friction coefficient of the coatings. From the response surface model, the MoS_2 target power has a stronger effect than the Ti target power on the friction coefficient and surface energy. MT coatings improved replication performance of the Si micromold and MT4 coated Si micromold showed better replication among all other coatings.

References

Barletta A, Gisario A, Tagliaferri V (2006) Electrostatic spray deposition (ESD) of polymeric powders on thermoplastic (PA66) substrate. Surf Coat Technol 201:296–308

Becker H, Heim U, Ieee I (1999) Silicon as tool material for polymer hot embossing, in Mems '99,In: twelfth ieee international conference on micro electro mechanical systems, technical digest. pp. 228–231

Benayoun S, Fouilland-Paille L, Hantzpergue JJ (1999) Microscratch test studies of thin silica films on stainless steel substrates. Thin Solid Films 352:156–166

Benjamin P, Weaver C (1960) Measurement of adhesion of thin films. Proc R Soc Lond Ser A 254:163–176

Dirckx M (2010) Demolding of hot embossed polymer microstructures, in Mechanical Engineering. Massachusetts institute of technology, Cambridge, MA

Donnet C (1996) Advanced solid lubricant coatings for high vacuum environments. Surf Coat Technol 80:151–156

Esch MB, Kapur S, Irizarry G, Genova V (2003) Influence of master fabrication techniques on the characteristics of embossed microfluidic channels. Lab Chip 3:121–127

Firouzi-Arani M, Savaloni H, Ghoranneviss M (2010) Dependence of surface nano-structural modifications of Ti implanted by N + ions on temperature. Appl Surf Sci 256:4502–4511

Fu G, Tor S, Loh N, Tay B, Hardt DE (2007) A micro powder injection molding apparatus for high aspect ratio metal microstructure production. J Micromech Microeng 17:1803–1809

Fu G, Tor SB, Loh NH, Tay BY, Hardt DE (2008) The demolding of powder injection molded micro-structures: analysis, simulation and experiment. J Micromech Microeng 18:075024

Gangopadhyay S, Acharya R, Chattopadhyay AK, Paul S (2009) Composition and structure-property relationship of low friction, wear resistant TiN-MoSx composite coating deposited by pulsed closed-field unbalanced magnetron sputtering. Surf Coat Technol 203:1565–1572

Gao JX, Yeo LP, Chan-Park MB, Miao JM, Yan YH, Sun JB, Lam YC, Yue CY (2006) Antistick postpassivation of high-aspect ratio silicon molds fabricated by deep-reactive ion etching. J Microelectromech Syst 15:84–93

Hilton MR, Fleischauer PD (1992) Applications of solid lubricant films in spacecraft. Surf Coat Technol 55:435–441

Hirai Y, Yoshida S, Okamoto A, Tanaka Y, Endo M, Irie S, Nakagawa H, Sasago M (2001) Mold surface treatment for imprint lithography. J Photopolym Sci Technol 14:457–462

Hirai Y, Yoshida S, Takagi N (2003) Defect analysis in thermal nanoimprint lithography. J Vac Sci Technol, B 21:2765–2770

Hsueh CH, Lee S, Lin HY, Chen LS, Wang WH (2006) Analyses of mechanical failure in nanoimprint processes. Mater Sci Eng, A 433:316–322

Ichimura H, Rodrigo A (2000) The correlation of scratch adhesion with composite hardness for TiN coatings. Surf Coat Technol 126:152–158

Jaszewski RW, Schift H, Schnyder B, Schneuwly A, Gröning P (1999) Deposition of anti-adhesive ultra-thin teflon-like films and their interaction with polymers during hot embossing. Appl Surf Sci 143:301–308

Kahraman S, Onal M, Sarikaya Y, Bozdogan I (2005) Characterization of silica polymorphs in kaolins by X-ray diffraction before and after phosphoric acid digestion and thermal treatment. Anal Chim Acta 552:201–206

Loke YW, Tor SB, Chun JH, Loh NH, Hardt DE (2007) Comparison between amorphous metallic alloy and silicon as molding insert for micro injection molding of polymers, 65th Ann. Tech. Conf.

& Exhibition, Society of Plastics Engineers, Cincinnati, OH, pp 6–11

Ma YY, Hu H, Northwood D, Nie XY (2007) Optimization of the electrolytic plasma oxidation processes for corrosion protection of magnesium alloy AM50 using the Taguchi method. J Mater Process Technol 182:58–64

Ma L, Xu LM, Xu XY, Luo YL, Chen WX (2009) Synthesis and characterization of flower-like MoS2 microspheres by a facile hydrothermal route. Mater Lett 63:2022–2024

Owens DK, Wendt RC (1969) Estimation of surface free energy of polymers. J Appl Polym Sci 13:1741–1747

Patton ST, Zabinski JS (2002) Failure mechanisms of a MEMS actuator in very high vacuum. Tribo Int 35:373–379

Radhakrishnan G, Robertson RE, Adams PM, Cole RC (2002) Integrated TiC coatings for moving MEMS. Thin Solid Films 420:553–564

Renevier NM, Lobiondo N, Fox VC, Teer DG, Hampshire J (2000a) Performance of MoS2/metal composite coatings used for dry machining and other industrial applications. Surf Coat Technol 123:84–91

Renevier NM, Fox VC, Teer DG, Hampshire J (2000b) Coating characteristics and tribological properties of sputter-deposited MoS2/metal composite coatings deposited by closed field unbalanced magnetron sputter ion plating. Surf Coat Technol 127:24–37

Rigato V, Maggioni G, Boscarino D, Sangaletti L, Depero L, Fox VC, Teer D, Santini C (1999) A study of the structural and mechanical properties of Ti-MoS2 coatings deposited by closed field unbalanced magnetron sputter ion plating. Surf Coat Technol 116:176–183

Rigato V, Maggioni G, Patelli A, Boscarino D, Renevier NM, Teer DG (2000) Properties of sputter-deposited MoS2/metal composite coatings deposited by closed field unbalanced magnetron sputter ion plating. Surf Coat Technol 131:206–210

Saha B, Liu E, Tor SB, Khun NW, Hardt DE, Chun JH (2009) Anti-sticking behavior of DLC-coated silicon micro-molds. J Micromech Microeng 19

Saha B, Liu E, Tor SB, Khun NW, Hardt DE, Chun JH (2010) Replication performance of Si-N-DLC-coated Si micro-molds in micro-hot-embossing, J Micromech Microeng 20

Saha B, Liu E, Tor SB, Hardt DE, Chun JH, Khun NW (2010) Improvement in lifetime and replication quality of Si micromold using N:DLC:Ni coatings for microfluidic devices, Sens. Actuators: B. Chemical, SNB 12473

Schift H (2008) Nanoimprint lithography: an old story in modern times? a review. J Vac Sci Technol, B 26:458–480

Smallwood SA, Eapen KC, Patton ST, Zabinski JS (2006) Performance results of MEMS coated with a conformal DLC. Wear 260:1179–1189

Spalvins T (1974) Structure of sputtered molybdenum-disulfide films at various substrate temperatures. Asle Trans 17:1–7

Stoldt CR, Bright VM (2006) Ultra-thin film encapsulation processes for micro-electro-mechanical devices and systems. J Phys D Appl Phys 39:R163–R170

Wilson GM, Sullivan JL (2007) The effects of pulsed substrate biasing on thin amorphous carbon coatings: a statistical design of experiment study. J Phys D Appl Phys 40:5438–5445

Xu J, Zhu MH, Zhou ZR, Kapsa P, Vincent L (2003) An investigation on fretting wear life of bonded MoS2 solid lubricant coatings in complex conditions. Wear 255:253–258

Yeo LP, Yan YH, Lam YC, Chan-Park MB (2006) Design of experiment for optimization of plasma-polymerized octafluoro-cyclobutane coating on very high aspect ratio silicon molds. Langmuir 22:10196–10203